
# ATLAS NOTE

ATL-PHYS-PUB-2015-018

23rd July 2015


# Track Reconstruction Performance of the ATLAS Inner Detector at $\sqrt{s} = 13$ TeV


The ATLAS Collaboration





## Abstract

This document summarizes the basic track reconstruction performance of the ATLAS inner detector using the first $\sqrt{s} = 13$ TeV data from proton-proton collisions collected at the LHC. It focuses on results obtained with the baseline track quality selection used within ATLAS. Track properties such as hits on track and measured impact parameter resolution are compared between data and simulation. The properties of hits on track are also studied in the core of jets. Overall, a good agreement between data and simulation is observed, while some discrepancies remain.

# 1 Introduction

For the first time the LHC has delivered proton-proton collisions at a center-of-mass energy of 13 TeV in 2015, the highest to date. This document shows the track reconstruction performance of the ATLAS inner detector [1] with the $\sqrt{s}$ = 13 TeV data, including a new detector: the IBL [2], which is described in Section 2. The used data is summarized in Section 3. Tracks are reconstructed by ATLAS's primary track reconstruction algorithm [3]. Two types of quality selections, described in more detail below, are applied; the so called loose selection and the tight-primary selection, which is for example applied to tracks used during vertex reconstruction. All quantities are compared to Monte Carlo (MC) simulated events. Among the comparisons are the hit content as well as more detailed performance measurements like the SCT and TRT extension efficiency, which are made in Section 4. Section 5 contains a measurement of the track impact parameter resolution and its comparison to simulation. The properties of hits on tracks in the core of high momentum jets are compared to MC simulation in Section 6.

# 2 The ATLAS Inner Detector and the Insertable B-Layer

The inner detector (ID) system (see Figure 1) which consists of a silicon pixel detector, a silicon microstrip detector (SCT) and the straw tubes of the transition radiation tracker (TRT), is used to measure the trajectories and momentum of charged particles in the region of $|\eta| < 2.5$.[1] The ID surrounds the beam pipe, and is located inside a solenoid magnet that provides a 2 T axial symmetric field.

A series of upgrades were made to ATLAS between run 1 and run 2, including improvements to the ID. In order to have better track and vertex reconstruction performance at the higher luminosities expected during run 2 and to mitigate the impact of radiation damage to the innermost layer of the pixel detector, a fourth layer, the insertable B-layer (IBL) [2] has been added to ATLAS. The IBL and a new beam pipe were installed in place of the original beam pipe inside the previous innermost pixel layer of the ID. The IBL consists of 14 staves instrumented with planar and 3D silicon pixel sensor technology along 332 mm on each side from the center of the ATLAS detector. The staves are arranged in turbine like fashion, with an overlap in $\phi$ and are mounted at an average radius of 35.7 mm.

[1] ATLAS uses a right-handed coordinate system with its origin at the nominal interaction point (IP) in the center of the detector and the $z$-axis along the beam pipe. The $x$-axis points from the IP to the center of the LHC ring, and the $y$-axis points upwards. Cylindrical coordinates $(r, \phi)$ are used in the transverse plane, $\phi$ being the azimuthal angle around the $z$-axis. The pseudorapidity is defined in terms of the polar angle $\theta$ as $\eta = -\ln\tan(\theta/2)$. Angular distance is measured in units of $\Delta R \equiv \sqrt{\Delta\eta^2 + \Delta\phi^2}$.

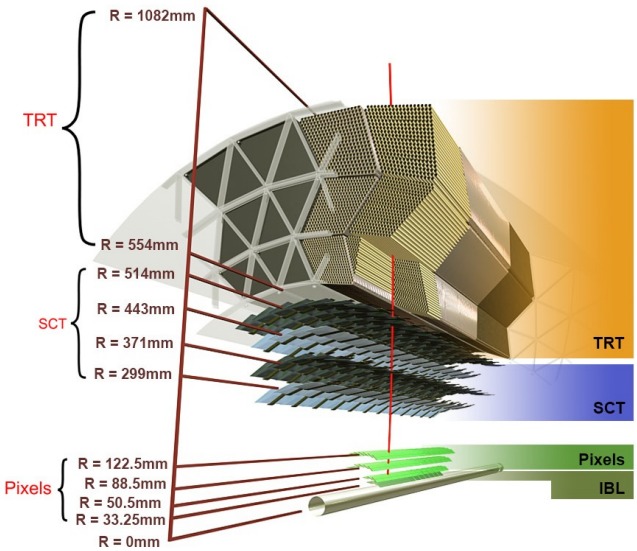


Figure 1: Sketch of the ATLAS inner detector showing all its components, including the new insertable B-layer (IBL). The distances to the interaction point are also shown.

## 3 Data-taking and Event selection

Data recorded during stable LHC running periods on June 9 and June 10 2015, when the tracking detectors and the solenoid were in fully operational mode, were used for Section 4 and 5. The LHC delivered collisions at low luminosity and the average number of interactions per bunch crossing, $\mu$, was about 0.005. Data from a second period, namely on June 13 and June 14 2015 when the LHC was delivering on average around 20 events per bunch crossing, were used in Section 6.

For the first period, inelastic proton-proton collisions were collected with a minimum-bias trigger, requiring at least one hit in the Minimum Bias Trigger Scintillators (MBTS) [4]. The MBTS located at $z = \pm 3.6$ m from the interaction point, has concentric inner and outer rings containing eight and four scintillating plates, respectively. The rings have an acceptance of $2.76 < |\eta| < 3.86$ (inner) and $2.08 < |\eta| < 2.76$ (outer). In total 10,838,000 events were recorded. Data for the first period is summarized in Table 1.

For the second period a single jet trigger with a threshold of 55 GeV on the transverse momentum, $p_{\mathrm{T}}$, was used to select events for this note. Jets within $|\eta| < 3.2$ are reconstructed from energy deposits forming topological clusters [5] of calorimeter cells using the anti-$k_t$ [6] algorithm with distance parameter $R = 0.4$. A total of 37,147,930 events were recorder for the second trigger selection.

Pythia 8.186 [7] is used in this note to generate events containing a single inelastic proton-proton interaction. The ATLAS minimum-bias tune A2 [8] is used, which is based on the MSTW2008LO PDF [9]. Only the non-diffractive component is used for the minimum-bias simulated data, which is used in Section 4 and 5. For Section 6, multi-jet processes are simulated using the Pythia 8.186 generator. The A14 tune is used together with the NNPDF2.3LO PDF set [10]. The EvtGen v1.2.0 program [11] is used for properties of the bottom and charm hadron decays.

The reconstructed track performance for the low luminosity run is presented for the loose and tight-primary track selection in events passing the following criteria:

- to fire a MBTS trigger on at least one side of the ATLAS detector.
- the presence of at least one reconstructed vertex with at least two tracks.
- the rejection of events with a second vertex containing four or more tracks, in order to remove events with more than one interaction per beam crossing.
- at least one track passing the loose selection.

For the high $\mu$ data used in Section 6, all events passing trigger selection and containing at least one reconstructed vertex are accepted.

**Track Selection** The used track selections are:

1. **Loose**, which requires:
   - $p_{\mathrm{T}} > 400$ MeV
   - $|\eta| < 2.5$
   - number of silicon hits $\geq 7$

- number of shared[2] modules $\leq 1$
- number of silicon holes[3] $\leq 2$
- number of pixel holes $\leq 1$

2. **Tight-Primary**, which requires on top of the loose selection:
   - number of silicon hits $\geq 9$ (if $|\eta| \leq 1.65$)
   - number of silicon hits $\geq 11$ (if $|\eta| > 1.65$)
   - either one IBL or next-to-innermost-pixel-layer hit
   - no pixel holes

Table 1: Summary of used data from low luminosity runs at $\sqrt{s} = 13$ TeV. The column $N_{\text{Evt}}$ represents the total number of events passing data quality and trigger selection. $N_{\text{Evt,sel}}$ represent the number of these events passing event selection, especially the requirement of one reconstructed vertex. $N_{\text{Trk}}$ is the total number of tracks in the selected events, while $N_{\text{Trk,loose}}$ and $N_{\text{Trk,tight}}$ are the tracks passing the loose and tight-primary selection respectively. A reconstruction setup specific for this low luminosity requirement was used for this data, reconstructing tracks down to a $p_{\text{T}}$ of 100 MeV. Therefore, most tracks fail selection because of the requirement on $p_{\text{T}}$ to be at least 400 MeV in the used track selections.

| Luminosity | $N_{\text{Evt}}$ | $N_{\text{Evt,sel}}$ | $N_{\text{Trk}}$ | $N_{\text{Trk,loose}}$ | $N_{\text{Trk,tight}}$ |
|---|---|---|---|---|---|
| 168 $\mu b^{-1}$ | 10 838 000 | 9 302 410 | 346 653 000 | 165 141 000 | 144 900 000 |

# 4 Basic Performance

In this section, data and simulation comparisons are illustrated for the loose track selection. The selected tracks in simulation are reweighted to ensure that their kinematics match those observed in data. The primary vertex z distribution in simulation is also matched to the data.

In Figure 2, the number of hits on track are compared for the individual detector technologies for tracks passing the loose track selection. Data and MC simulation agree well for all quantities. A similar comparison of the average number of hits versus $\eta$ is shown in Figure 3. The remaining discrepancies can be attributed to multiple sources. The dominant ones are wrong descriptions of dead and inefficient pixel modules in the MC simulation and residual mis-alignment of the detector elements of the ID [12]. Especially, the asymmetry observed in Figure 3(a) can be attributed to dead modules in one of the runs used. This is demonstrated in Figure 4, where as in Figure 3(b) the average number of pixel hits versus $\eta$ is shown, but the description of dead and inefficient pixel modules in simulation has been adjusted to match the one in the corresponding data set.

[2] A shared module, is either a hit in the pixel detector which is used by more than one track, or in the case of the SCT two shared hits in the same SCT layer.

[3] Holes are defined as intersections of the reconstructed track trajectory with a sensitive detector element that do not result in a hit. These are estimated by following closely the track trajectory and comparing the hits-on-track with the intersected modules. Inactive modules or regions such as edge areas on the silicon sensors are excluded from the hole definition.

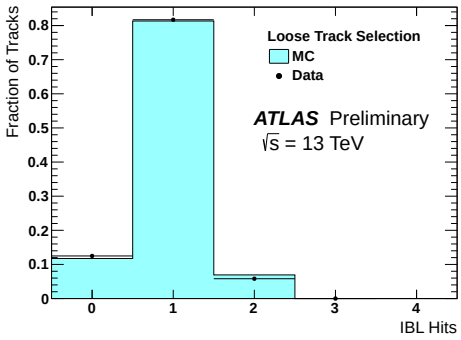


(a) Number of IBL Hits

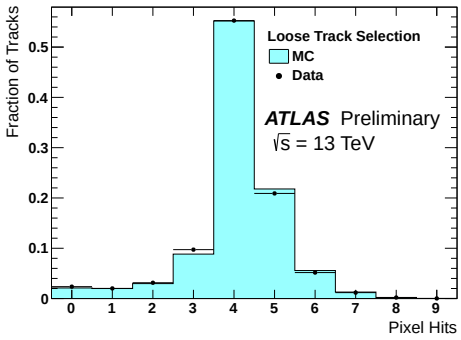


(b) Number of Pixel Hits

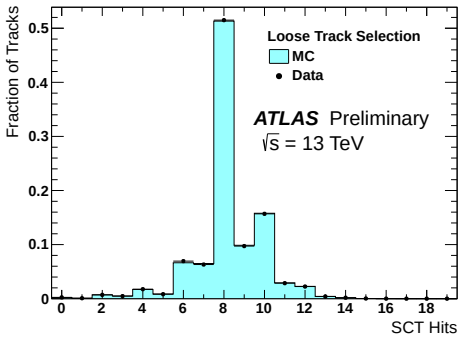


(c) Number of SCT Hits

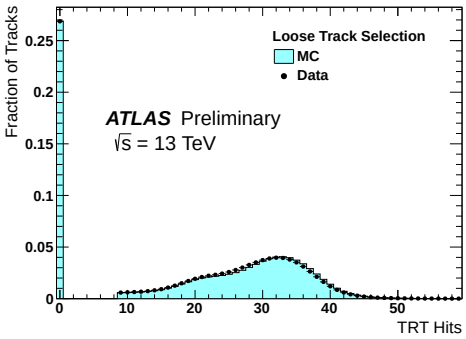


(d) Number of TRT Hits

Figure 2: Comparison of the number of (a) IBL, (b) pixel, (c) SCT and (d) TRT hits distributions in data and simulation (PYTHIA 8 A2:MSTW2008LO) for the loose track selection. The distributions are normalized to one.

The efficiency to extend a track to the SCT, i.e. to add hits from the SCT to a track with only pixel hits, is presented in Figure 5(a). For this plot different track selection criteria are applied, specifically the track to be extended into the SCT is required to have a minimum of four pixel hits. For the extension to be successful it is required to have at least two SCT hits on the extended track. Similarly, the efficiency to extend a track with silicon hits into the TRT is shown in Figure 5(b) for both the loose and tight-primary selections. A successful extension into the TRT requires at least nine TRT hits to be added to the track. While both of the efficiencies are affected by the amount of material between the respective detector volumes, this effect dominates for the SCT extension efficiency. This makes it a good quantity to check for differences in the detector description between data and simulation. The observed discrepancies are rather small and agree with the uncertainty expected from the material description.

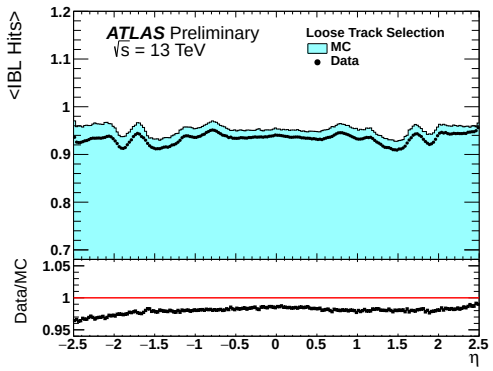


(a) Average number of IBL Hits vs $\eta$

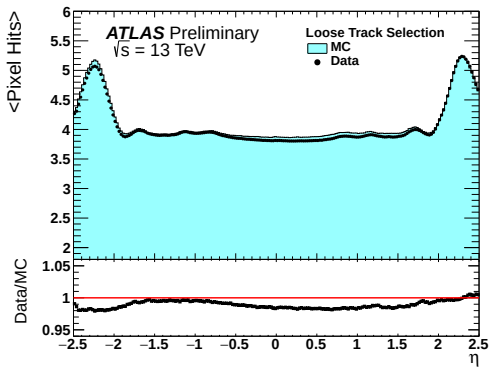


(b) Average number of Pixel Hits vs $\eta$

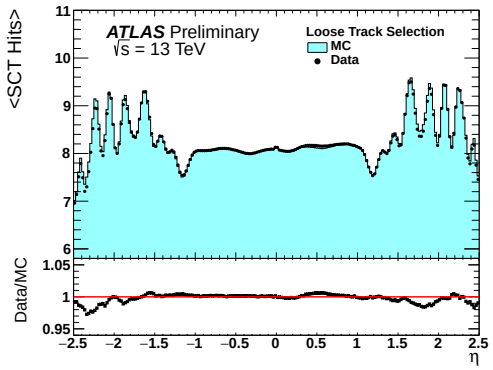


(c) Average number of SCT Hits vs $\eta$

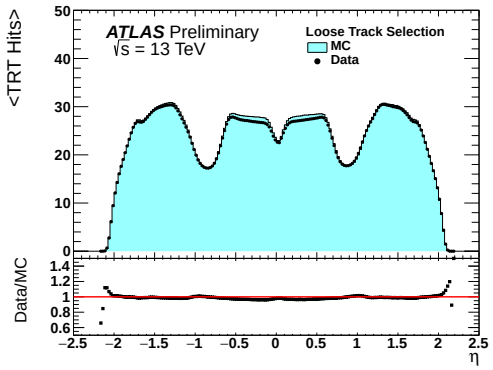


(d) Average number of TRT Hits vs $\eta$

Figure 3: Comparison of the average number of (a) IBL, (b) pixel, (c) SCT and (d) TRT hits per selected track as a function of pseudorapdity of the track in data and simulation for the loose track selection.

# 5 Track Parameter Resolution

The primary vertex[4] is in the following used as reference point to measure the impact parameter. Figure 6 shows the transverse and longitudinal impact parameters in data and simulation for tracks passing the loose track selection. A subset of the previously discussed data from low $\mu$ runs at $\sqrt{s} = 13$ TeV is used. The loose track selection is applied. The simulation again is reweighted to take into account the $(p_T, \eta)$ kinematics of tracks, as well as the $z$-vertex distribution in data. The observed differences in Figure 6(a) arise from discrepancies in the material description used in simulation for the IBL, a effect dominant at low $p_{\mathrm{T}}$. At higher $p_{\mathrm{T}}$, also the residual misalignment of the detector components contributes to the discrepancy. The impact parameter resolution is driven by the resolution of the individual measurements in the pixel detector. In simulation, the resolution of the longitudinal measurements is known to be superior to that in data due to a simplified energy deposit model. This effect is visible in Figure 6(b).

Since the impact parameter is measured with respect to the primary vertex, the resolution of the primary

[4] The primary vertex is defined as the one with the highest sum of $p_{\mathrm{T}}$ of tracks associated to it.

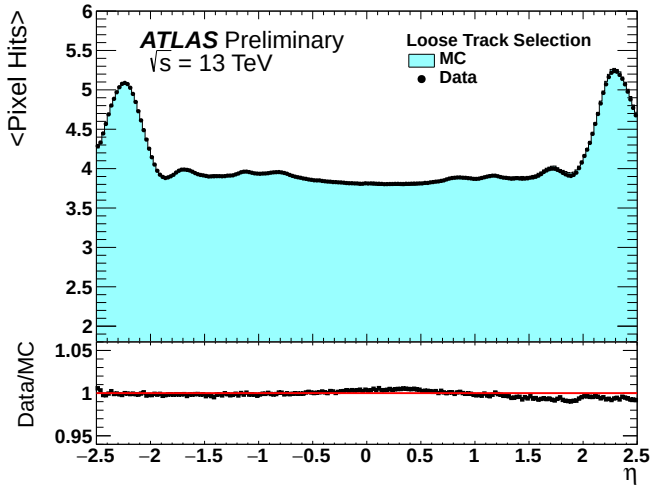


Figure 4: Comparison of the average number of pixel hits per selected track as a function of pseudorapdity of the track in data and simulation for the loose track selection. The Monte Carlo simulation uses an updated description of dead and inefficient modules derived specifically for the data set which is plotted.

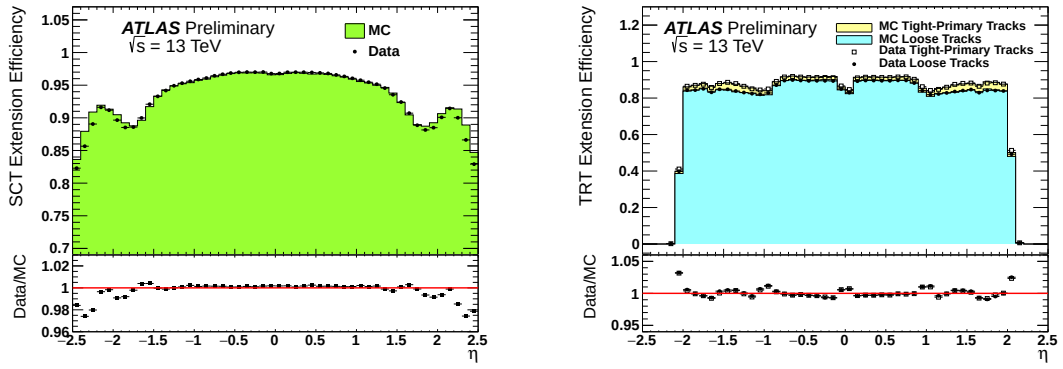


(a) SCT Extension Efficiency

(b) TRT Extension Efficiency

Figure 5: Efficiency to extend a track reconstructed in the pixel detector to the (a) SCT and the efficiency to extend a track reconstructed in the silicon detectors to the (b) TRT in data and simulation.

vertex is unavoidably folded into the impact parameter's intrinsic resolution. Moreover, even the unbiased[5] primary vertex resolution depends on the $p_{\mathrm{T}}$ and $\eta$ of the track in question, due to the correlations of this track with the remaining tracks present in the same event – though this is a minor effect. As the impact parameter resolution depends on the tracks kinematics, its distribution is further convolved as a function of $p_{\mathrm{T}}$ and $\eta$. For a proper comparison between data and simulation the impact parameter resolution needs to be unfolded from the resolution of its reference point. This iterative deconvolution procedure is described elsewhere [13]. It was validated by comparing the unfolded resolution in simulation to the one known for

[5] The unbiased resolution of a vertex measurement can be obtained by removing a specific track from the inputs used to determine the vertex's position and then recalculating it.

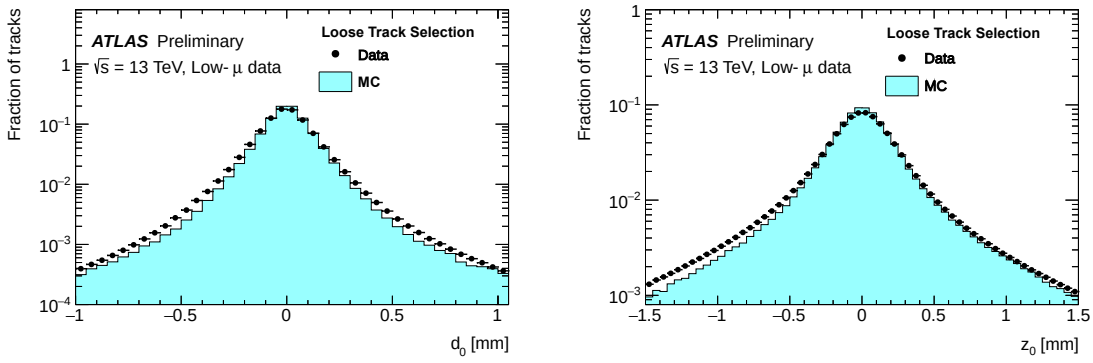


(a) Transverse

(b) Longitudinal

Figure 6: (a) Transverse, $d_0$, and (b) longitudinal, $z_0$, impact parameter distributions expressed with respect to the primary vertex. The average number of interactions per bunch crossing, $\mu$, for the used data set was about 0.005.

the generated particles and was shown to be in general in agreement with the intrinsic resolution. In the unfolded $z_0$ resolution a discrepancy can be observed for tracks above $|\eta| \sim 0.5$. This residual discrepancy is added as a systematic error to the MC simulation in the comparison below.

The results of this unfolding can be seen in Figure 7. The results from data are plotted alongside the values expected for particles from simulation. In both Figures 7(a) and 7(c) a more or less constant difference from low to higher $p_{\mathrm{T}}$ is observed in a central $\eta$ region of $0.2 < \eta < 0.4$, which accounts for roughly a 16% and 5% worsened resolution of $d_0$ and $z_0$ respectively. At high $\eta$, the $z_0$ resolution differs vastly from the expected value, as visible in Figure 7(d). For the $d_0$, this behavior can not be observed, but it rather shows a 15−20% difference in the selected $p_{\mathrm{T}}$ range. The source of this differences was already discussed for Figure 6.

## 6 Tracks in Jets

The properties of pixel and IBL hits on tracks inside the cones of reconstructed jets are compared between data and simulation in this section. This is done as a function of $\Delta R$(jet,track), the separation between the track and the jet axis. Jets are reconstructed from energy deposits forming topological clusters [5] of calorimeter cells using the anti-$k_t$ algorithm with distance parameter $R = 0.4$. Only tracks, passing the loose selection, inside the cone of jets with a $p_{\mathrm{T}} > 150$ GeV are considered in this section. For this, tracks are associated to the calorimeter jets following the ghost association procedure [14]. The simulation is reweighted to make sure that the average interactions per bunch crossing and the jet $\eta$ spectra match those in data. Besides considering the average number of pixel and IBL hits on track as a function of the track's distance to the jet axis, the main interest lies in the average number of shared and split hits. A hit is considered split if during the so called ambiguity solving stage [15] of the track reconstruction it was identified as being created by multiple charged particles. This is done with the help of an artificial neural network, mainly based on the shape and the amount of deposited charge in the hit [16]. If a hit is on more than one reconstructed track, and not already marked as split, it is considered shared.

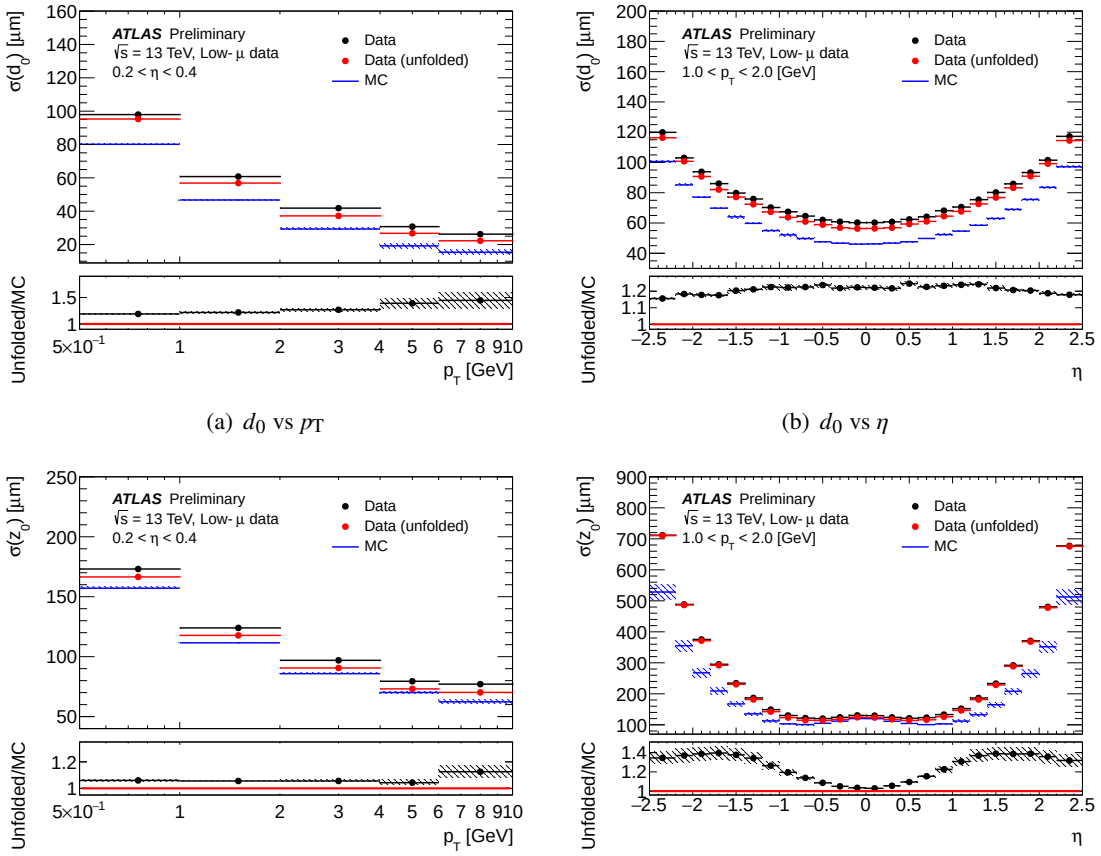


(a) $d_0$ vs $p_{\mathrm{T}}$

(b) $d_0$ vs $\eta$

(c) $z_0$ vs $p_{\mathrm{T}}$

(d) $z_0$ vs $\eta$

Figure 7: Unfolded (a,b) transverse and (c,d) longitudinal impact parameter resolution measured in data as a function of $p_{\mathrm{T}}$ (for values of $0.2 < \eta < 0.4$) and $\eta$ (for values of $1 < p_{\mathrm{T}} < 2$ GeV), compared to the expectation from Monte Carlo simulation. The error on Monte Carlo simulation includes the statistical uncertainty and the non-closure of unfolded Monte Carlo data with respect to the true resolution known from simulation. For reference, all figures also show the resolution in data before unfolding. The average number of interactions per bunch crossing, $\mu$, for the used data set was about 0.005.

Figure 8 shows the number of pixel and IBL hits on track versus $\Delta R$(jet,track). The simulation nicely reproduces the observed distribution from data. The number of split IBL hits, see Figure 9(a), shows reasonable agreement between data and simulation, which is a good indicator that the artificial neural network used shows a similar response in both. Relative differences of up to 15% remain for tracks in the very core of jets, at $\Delta R$(jet,track) $< 0.05$. A good agreement is observed for the number of shared IBL hits, as shown in Figure 9(b). This points to the track reconstruction performing as expected in data for the core of jets.

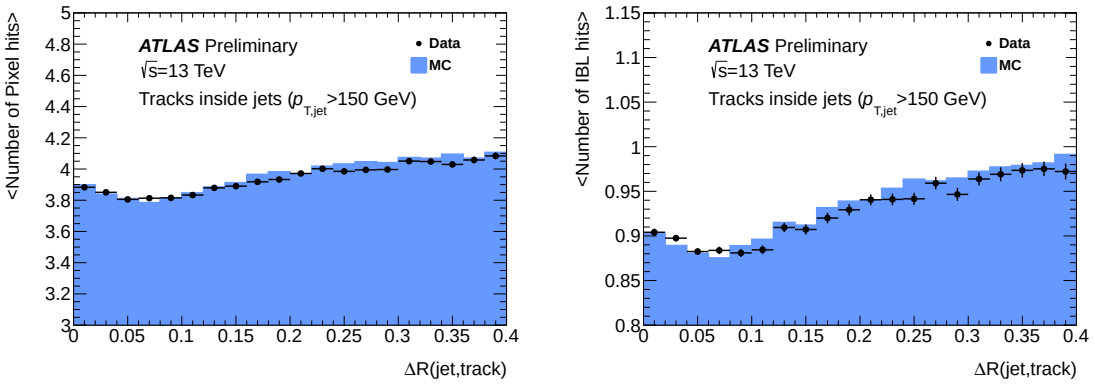


(a) Pixel (b) IBL

Figure 8: The number of (a) pixel and (b) IBL hits on track as a function of ΔR(jet,track) in data and simulation. Only tracks inside jets with a $p_T > 150$ GeV are selected.

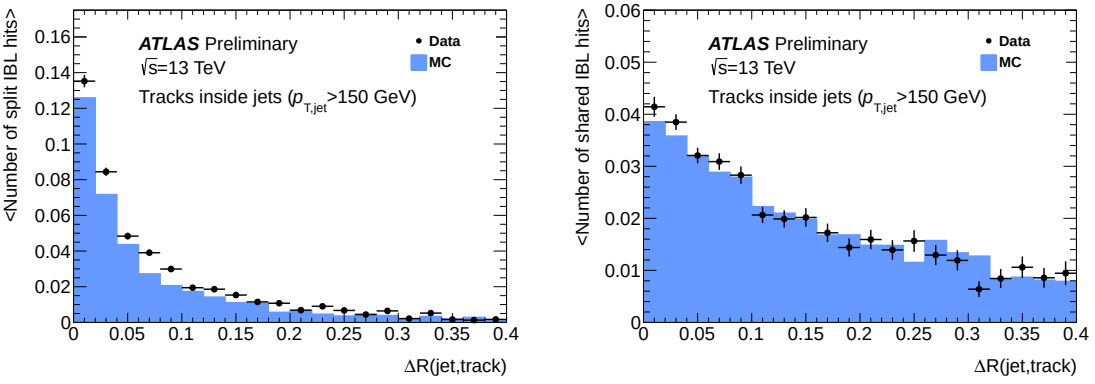


(a) Split hits (b) Shared hits

Figure 9: The number of (a) split and (b) shared IBL hits on track as a function of ΔR(jet,track) in data and simulation. Split hits are identified as originating from more than one track by an artificial neural network during the reconstruction. Shared hits are used by more than one track and are not identified as split. Only tracks inside jets with a $p_T > 150$ GeV are selected.

## References


[1] ATLAS Collaboration, *The ATLAS Experiment at the CERN Large Hadron Collider*, JINST **3** (2008) S08003, URL: http://stacks.iop.org/1748-0221/3/i=08/a=S08003.

[2] ATLAS Collaboration, *ATLAS Insertable B-Layer Technical Design Report*, CERN-LHCC-2010-013. ATLAS-TDR-19 (2010), URL: https://cds.cern.ch/record/1291633; ATLAS Collaboration, *ATLAS Insertable B-Layer Technical Design Report Addendum*, CERN-LHCC-2012-009. ATLAS-TDR-19-ADD-1 (2012), URL: https://cds.cern.ch/record/1451888.

[3] ATLAS Collaboration, *Concepts, Design and Implementation of the ATLAS New Tracking (NEWT)*, ATL-SOFT-PUB-2007-007 (2007), URL: https://cds.cern.ch/record/1020106.

[4] A. Sidoti on behalf of the ATLAS TDAQ Collaboration, *Minimum Bias Trigger Scintillators in ATLAS Run II*, Journal of Instrumentation **9**.10 (2014) C10020, URL: http://stacks.iop.org/1748-0221/9/i=10/a=C10020.

[5] ATLAS Collaboration, *Calorimeter Clustering Algorithms: Description and Performance*, ATL-LARG-PUB-2008-002 (2008), URL: https://cds.cern.ch/record/1099735.

[6] M. Cacciari, G. P. Salam and G. Soyez, *The anti-$k_t$ jet clustering algorithm*, Journal of High Energy Physics **2008**.04 (2008) 063, URL: http://stacks.iop.org/1126-6708/2008/i=04/a=063.

[7] T. Sjostrand, S. Mrenna and P. Z. Skands, *A Brief Introduction to PYTHIA 8.1*, Comput.Phys.Commun. **178** (2008) 852–867, arXiv: 0710.3820 [hep-ph].

[8] ATLAS Collaboration, *Further ATLAS tunes of PYTHIA6 and Pythia 8*, ATL-PHYS-PUB-2011-014 (2011), URL: https://cds.cern.ch/record/1400677.

[9] A. Sherstnev and R. Thorne, *Parton Distributions for LO Generators*, Eur.Phys.J. **C55** (2008) 553–575, arXiv: 0711.2473 [hep-ph].

[10] R. D. Ball et al., *Parton distributions with LHC data*, Nucl. Phys. **B867** (2013) 244–289, arXiv: 1207.1303 [hep-ph].

[11] D. J. Lange, *The EvtGen particle decay simulation package*, Nucl. Instrum. Meth. **A462** (2001).

[12] ATLAS Collaboration, *Alignment of the ATLAS Inner Detector with the initial LHC data at $\sqrt{s}$ = 13 TeV*, ATL-PHYS-PUB-2015-031 (2015), URL: https://atlas.web.cern.ch/Atlas/GROUPS/PHYSICS/PUBNOTES/ATL-PHYS-PUB-2015-031/.

[13] ATLAS Collaboration, *Tracking Studies for b-tagging with 7 TeV Collision Data with the ATLAS Detector*, ATLAS-CONF-2010-070 (2010), URL: https://cds.cern.ch/record/1281352.

[14] M. Cacciari, G. P. Salam and G. Soyez, *The catchment area of jets*, Journal of High Energy Physics **2008**.04 (2008) 005, URL: http://stacks.iop.org/1126-6708/2008/i=04/a=005.

[15] ATLAS Collaboration, *The Optimization of ATLAS Track Reconstruction in Dense Environments*, ATL-PHYS-PUB-2015-006 (2015), URL: https://cds.cern.ch/record/2002609.

[16] ATLAS Collaboration,
*A neural network clustering algorithm for the ATLAS silicon pixel detector*,
JINST **9** (2014) P09009, URL: http://stacks.iop.org/1748-0221/9/i=09/a=P09009.